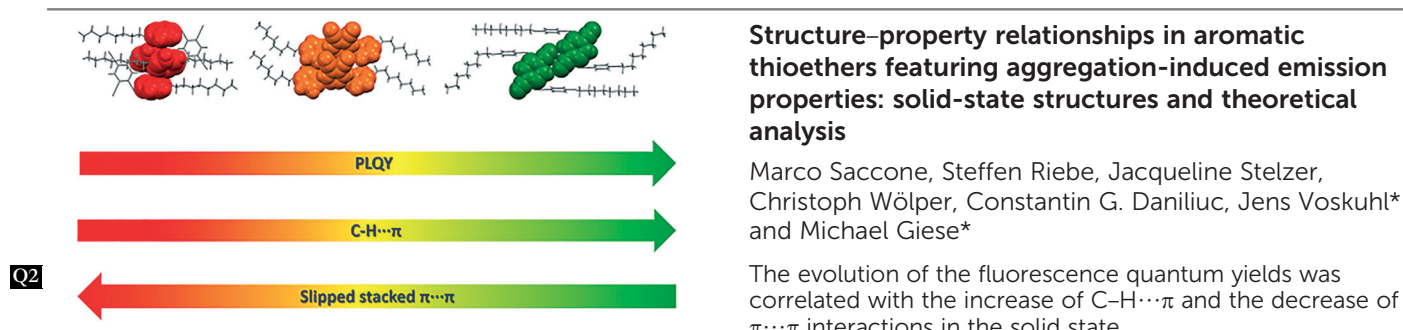


We have presented the Graphical Abstract text and image for your article below. This brief summary of your work will appear in the contents pages of the issue in which your article appears.



Please check this proof carefully. Our staff will not read it in detail after you have returned it.

Please send your corrections either as a copy of the proof PDF with electronic notes attached or as a list of corrections. **Do not edit the text within the PDF or send a revised manuscript** as we will not be able to apply your corrections. Corrections at this stage should be minor and not involve extensive changes.

**Proof corrections must be returned as a single set of corrections, approved by all co-authors. No further corrections can be made after you have submitted your proof corrections as we will publish your article online as soon as possible after they are received.**

Please ensure that:

- The spelling and format of all author names and affiliations are checked carefully. You can check how we have identified the authors' first and last names in the researcher information table on the next page. **Names will be indexed and cited as shown on the proof, so these must be correct.**
- Any funding bodies have been acknowledged appropriately and included both in the paper and in the funder information table on the next page.
- All of the editor's queries are answered.
- Any necessary attachments, such as updated images or ESI files, are provided.

Translation errors can occur during conversion to typesetting systems so you need to read the whole proof. In particular please check tables, equations, numerical data, figures and graphics, and references carefully.

Please return your **final** corrections, where possible within **48 hours** of receipt, by e-mail to: [crystengcomm@rsc.org](mailto:crystengcomm@rsc.org). If you require more time, please notify us by email.

## Funding information

Providing accurate funding information will enable us to help you comply with your funders' reporting mandates. Clear acknowledgement of funder support is an important consideration in funding evaluation and can increase your chances of securing funding in the future.

We work closely with Crossref to make your research discoverable through the Funding Data search tool (<http://search.crossref.org/funding>). Funding Data provides a reliable way to track the impact of the work that funders support. Accurate funder information will also help us (i) identify articles that are mandated to be deposited in **PubMed Central (PMC)** and deposit these on your behalf, and (ii) identify articles funded as part of the **CHORUS** initiative and display the Accepted Manuscript on our web site after an embargo period of 12 months.

Further information can be found on our webpage (<http://rsc.li/funding-info>).

### What we do with funding information

We have combined the information you gave us on submission with the information in your acknowledgements. This will help ensure the funding information is as complete as possible and matches funders listed in the Crossref Funder Registry.

If a funding organisation you included in your acknowledgements or on submission of your article is not currently listed in the registry it will not appear in the table on this page. We can only deposit data if funders are already listed in the Crossref Funder Registry, but we will pass all funding information on to Crossref so that additional funders can be included in future.

### Please check your funding information

The table below contains the information we will share with Crossref so that your article can be found *via* the Funding Data search tool. **Please check that the funder names and grant numbers in the table are correct and indicate if any changes are necessary to the Acknowledgements text.**

Funder name	Funder's main country of origin	Funder ID (for RSC use only)	Award/grant number
-------------	---------------------------------	------------------------------	--------------------

## Researcher information

Please check that the researcher information in the table below is correct, including the spelling and formatting of all author names, and that the authors' first, middle and last names have been correctly identified. **Names will be indexed and cited as shown on the proof, so these must be correct.**

If any authors have ORCID or ResearcherID details that are not listed below, please provide these with your proof corrections. Please ensure that the ORCID and ResearcherID details listed below have been assigned to the correct author. Authors should have their own unique ORCID iD and should not use another researcher's, as errors will delay publication.

Please also update your account on our online [manuscript submission system](#) to add your ORCID details, which will then be automatically included in all future submissions. See [here](#) for step-by-step instructions and more information on author identifiers.

First (given) and middle name(s)	Last (family) name(s)	ResearcherID	ORCID
Marco	Saccone	B-2522-2015	0000-0002-1768-0028
Steffen	Riebe		
Jacqueline	Stelzer		
Christoph	Wölper		
Constantin G.	Daniliuc		0000-0002-6709-3673
Jens	Voskuhl		0000-0002-9612-2306
Michael	Giese		0000-0001-6355-536X

## Queries for the attention of the authors

Journal: **CrystEngComm**

Paper: **c9ce00444k**

Title: **Structure–property relationships in aromatic thioethers featuring aggregation-induced emission properties: solid-state structures and theoretical analysis**

For your information: You can cite this article before you receive notification of the page numbers by using the following format: (authors), CrystEngComm, (year), DOI: 10.1039/c9ce00444k.

Editor's queries are marked on your proof like this **Q1**, **Q2**, etc. and for your convenience line numbers are indicated like this 5, 10, 15, ...

Please ensure that all queries are answered when returning your proof corrections so that publication of your article is not delayed.

Query Reference	Query	Remarks
Q1	Please confirm that the spelling and format of all author names is correct. Names will be indexed and cited as shown on the proof, so these must be correct. No late corrections can be made.	
Q2	Please check that the Graphical Abstract text fits within the allocated space indicated on the front page of the proof. If the entry does not fit between the two horizontal lines, then please trim the text and/or the title.	
Q3	Please check that the inserted CCDC numbers are correct.	
Q4	Do you wish to add an e-mail address for the corresponding author? If so, please provide the relevant information.	
Q5	The meaning of the word “periodicize” in the sentence beginning “Finally it is...” is not clear - please provide alternative text.	
Q6	The sentence beginning “The interaction energy...” has been altered for clarity, please check that the meaning is correct.	
Q7	The sentence beginning “More rigorous arguments...” has been altered for clarity, please check that the meaning is correct.	
Q8	In the sentence beginning “In Fig. 7 another...” there is a citation to Fig. 4C, however Fig. 4 does not appear to contain a part (C). Please resupply the figure (preferably as a TIF file at 600 dots per inch) or amend the text accordingly.	

# Structure–property relationships in aromatic thioethers featuring aggregation-induced emission properties: solid-state structures and theoretical analysis†

Cite this: DOI: 10.1039/c9ce00444k

Marco Saccone,<sup>a</sup> Steffen Riebe,<sup>a</sup> Jacqueline Stelzer,<sup>a</sup> Christoph Wölper,<sup>b</sup> Constantin G. Daniliuc,<sup>c</sup> Jens Voskuhl<sup>\*a</sup> and Michael Giese<sup>id</sup><sup>\*a</sup>

Received 25th March 2019,  
Accepted 15th April 2019

DOI: 10.1039/c9ce00444k

rsc.li/crystengcomm

We describe in this paper a structure–property relationship study of aromatic thioethers with aggregation-induced emission (AIE) properties. We combine a structural analysis based on geometrical consideration with an in-depth analysis of the crystalline packing supported by quantum mechanical calculations. Our results allow us to correlate the enhanced fluorescence quantum yields with the significant increase of C–H⋯π and the decrease of π⋯π interactions in the solid state – a result which supports the well-accepted AIE mechanism quantitatively.

## Introduction

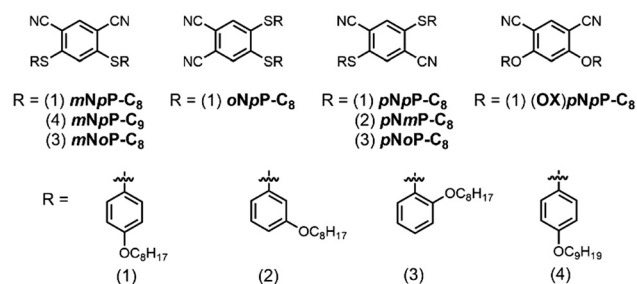
The design, synthesis and analysis of organic materials, showing highly effective and tuneable emission in the solid state, are cutting-edge topics in research due to their importance in fields such as optoelectronics and materials sciences.<sup>1</sup> The combination of self-assembly and tailored luminescence properties is especially challenging, since self-assembly often goes along with strong secondary interactions involving π–π stacking, besides more specific directional interactions, such as hydrogen and halogen bonding,<sup>2</sup> which leads to non-radiative charge-transfer complexes and thus quenching of fluorescence.<sup>3</sup> One approach to overcome this behaviour is the use of a phenomenon which was first described in 2001 by the group of Tang.<sup>4</sup> The so-called aggregation-induced emission (AIE) uses luminophores behaving in contrast to classic emitters, which are typically quenched upon aggregation. Here compounds which exhibit a rotor-like structure are capable of showing high rotational mobility in organic solvent converting absorbed light into motion, which goes along with a loss in emission. Upon aggregation, a restriction of the intramolecular motion (RIM) or rotation (RIR) is achieved leading to classic fluorophores or phosphors, with increased quantum yields.<sup>5</sup> Recently, Voskuhl and co-workers proposed a

new class of AIE fluorophores based on aromatic thioethers, which are synthetically easy to access without costly purification processes.<sup>6</sup> Furthermore, the emission wavelength can be easily tuned by variations of the substitution pattern as well as the introduction of different functional groups. In the last decade significant progress has been made in order to understand the mechanism of AIE.<sup>1</sup> Herein, we report a comprehensive analysis of the crystal structures of aromatic thioethers featuring AIE properties<sup>7</sup> in order to obtain deep insight into the intermolecular interactions which govern the crystal packing and influence the emission behaviour. Therefore, a careful theoretical investigation of the intermolecular forces is reported together with the solid state analysis, which will shed new light on the solid state properties of molecules with AIE.

## Methods

### Materials design

The schematic structures of the aromatic thioethers featuring AIE are depicted in Scheme 1.



**Scheme 1** Chemical structure of the molecules considered in the present study.

<sup>a</sup> Institute of Organic Chemistry, University of Duisburg Essen, Universitätsstraße 7, Essen 45141, Germany

<sup>b</sup> Institute of Inorganic Chemistry, University of Duisburg Essen, Universitätsstraße 7, Essen 45141, Germany

<sup>c</sup> Institute of Organic Chemistry Westfälische Wilhelms-Universität Münster, Corrensstrasse 40, 48149 Münster, Germany

† Electronic supplementary information (ESI) available. CCDC 1893331, 1894901, 1895359, 1895360 and 1895424. For ESI and crystallographic data in CIF or other electronic format see DOI: 10.1039/c9ce00444k

The synthesis and characterization of their photochemistry were reported earlier and are summarized in the ESI.†<sup>7</sup> Herein, we report five new crystal structures, namely *mNpP-C<sub>9</sub>* (with linear C<sub>9</sub>H<sub>19</sub> chains, in place of the C<sub>8</sub>H<sub>17</sub> chains), *mNoP-C<sub>8</sub>*, *pNmp-C<sub>8</sub>*, *pNoP-C<sub>8</sub>* and the ether (O in place of S) analogue of *mNpP-C<sub>8</sub>*, which we call here (Ox)*mNpP-C<sub>8</sub>*. In addition to that, the previously reported structures of *mNpP-C<sub>8</sub>*, *oNpP-C<sub>8</sub>* and *pNpP-C<sub>8</sub>* are discussed and compared to the new structures. Furthermore, a comprehensive analysis of the intra- and intermolecular packing is reported to understand the AIE behaviour. Crystallographic data collection and details are shown in the ESI.†

### Theoretical background and computational aspects

Besides the description of the crystal structures, the main goal of the present manuscript is to derive structure–property relationships from the analysis of intermolecular forces in crystalline solids. Due to the size of our systems (molecules of about 100 atoms) we assume pairwise additivity, *i.e.* we assume that the energy of the system can be approximated as a sum of interaction energies between pairs of molecules:

$$W = \sum_i W_i + \sum_{i>j} E_{ij}$$

where  $W_i$  is the energy of the isolated molecule  $i$ , and  $E_{ij}$  is the interaction energy between the pair  $i$  and  $j$  taken in the absence of other molecules but in the geometry that they have in the whole system.<sup>8</sup> This approximation is usually excellent for systems such as noble gases and hydrocarbon molecules (our case).<sup>9</sup> It also performs well for weak to moderate hydrogen bonds. However, it is not suitable for the description of strongly interacting systems such as metal clusters.<sup>10</sup> Seminal examples of such calculations were discussed recently.<sup>11</sup> Methodologies for partitioning the interaction energies such as SAPT were also developed.<sup>12</sup> Finally it is worth mentioning that the proper way of dealing with crystalline systems is to periodicize the orbital representation of the system, and this methodology is being pursued by different collaborations around the world.<sup>13</sup> These wavefunction-based, periodic, or SAPT calculations are prohibitively expensive if applied to systems containing hundreds of atoms, and the results are heavily dependent on the choice of the basis set and the method for introducing the electron correlation.<sup>14</sup> In the present study we use a semi-empirical approach, popularized by Gavezzotti with the PIXEL method<sup>15</sup> and recently revamped by Spackman *et al.*, who developed the CrystalExplorer<sup>16</sup> suite, which we used here. The interaction energy is decomposed into a sum of the following terms,

$$E_{\text{tot}} = E_{\text{ele}} + E_{\text{pol}} + E_{\text{dis}} + E_{\text{rep}}$$

which were already discussed by Gavezzotti<sup>15</sup> and explained in detail by Turner *et al.* in their implementation.<sup>17</sup> Monomer electron densities used to compute  $E_{\text{ele}}$ ,  $E_{\text{pol}}$ , and  $E_{\text{rep}}$  were obtained at the B3LYP/6-31G(d,p) level of theory, and  $E_{\text{rep}}$  is

the Grimme D3 dispersion correction, summed over all intermolecular atom pairs. Geometries were taken from crystallographic coordinates. Before starting the calculations, X–H distances were normalized to the values obtained from neutron diffraction studies of small molecules. It has been shown that interaction energies<sup>17</sup> and lattice parameters<sup>18</sup> computed with CrystalExplorer are in excellent agreement with those obtained by means of highly accurate but prohibitively costly wavefunction methods, which were used to prepare the benchmarks reported in 2016.<sup>11</sup>

## Results and discussion

### Description of the solid-state structures

The molecules of *pNoP-C<sub>8</sub>* are connected by the non-classical hydrogen bond C12–H12a⋯N1 (see Fig. S1, ESI†) and a C⋯ $\pi$  interaction between the nitrile group and the central phenyl ring. This leads to the formation of chains parallel to the  $a$ -axis, showing short S⋯ $\pi$  contacts. The chains form layers *via* a non-classical hydrogen bond (H7⋯N1) which are oriented parallel to (001). The core of the layer consists of the polar part of the molecules, while the non-polar alkyl chains are located in the periphery of the layer. Two CH⋯CH contacts support the proximity of aliphatic chains of neighbouring molecules, namely C12–H12b⋯H14b–C14 and C11–H11a⋯H13b–C13 (Fig. 1).

In analogy with what we observed in *pNoP-C<sub>8</sub>*, a non-classical hydrogen bond C8–H8⋯N1 connects the molecules of *pNmp-C<sub>8</sub>* (Fig. S2, ESI†). This leads to the formation of chains parallel to  $a$ . In *pNmp-C<sub>8</sub>* some intra-chain  $\pi$ ⋯ $\pi$  interactions occur due to the close proximity of the carbon atoms of the nitrile moieties, namely C1⋯C2 contacts. Other intra-chain CH⋯ $\pi$  interactions involve C11–H11b and C12–H12a contacts with the benzene ring containing C5, C6 and C10 (Fig. 2).

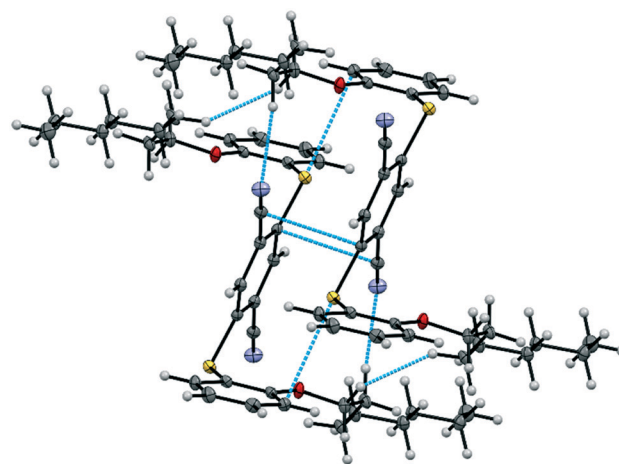


**Fig. 1** Partial intermolecular landscape of *pNoP-C<sub>8</sub>* (CCDC Nr.: 1895360). Blue lines represent short intermolecular contacts below the sum of the van der Waals radii of the respective atoms. Color chart: grey = C, white = H, red = O, purple = N, and yellow = S. Ellipsoids are shown at the 50% probability level.

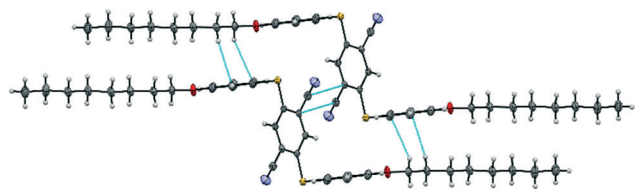


Fig. 2 Partial intermolecular landscape of *pNpP-C<sub>8</sub>* (CCDC Nr.: 1895359). Blue lines represent short intermolecular contacts below the sum of the van der Waals radii of the respective atoms. Color chart: grey = C, white = H, red = O, purple = N, and yellow = S. Ellipsoids are shown at the 90% probability level.

The molecules of *mNoP-C<sub>8</sub>* form dimers *via* CH $\cdots$ N hydrogen bonds from the central ring to the nitrile group. These dimers form centres of inversion thus an annular motif is formed (see Fig. 3). The dimers are connected by further non-classical hydrogen bonds to strings parallel to [111]. The surface of the strings is dominated by the alkyl chains and no crosslinking by oriented interactions can be found.

In contrast to the structure of *mNpP-C<sub>8</sub>* with the C8 alkyl chain, the *mNpP-C<sub>9</sub>* compound shows a hairpin-like conformation with weak intra-molecular  $\pi\cdots\pi$  interactions between the two residual phenyl rings with the shortest distance between the carbon atoms C15 $\cdots$ C24 of 3.565 Å and an interplanar angle of the phenyl rings of 26.4° (Fig. S3, ESI†). The packing presents two major motifs. The first one shows short N $\cdots\pi$  interactions involving the nitrile group and the main phenyl ring of the neighbouring molecules (N1 $\cdots$ Cg1 2.960 Å, with the Cg1 centroid of C3/C4/C8 atoms) sustained by an additional CH $\cdots$ S interaction (C22–H2 $\cdots$ S1 3.097 Å; 138.6°) between the sulphur and the residual phenyl ring. These interactions are related by the *b* glide plane (Fig. S4, ESI†). The second motif contains a mixture of three types of non-classical hydrogen bonds involving the nitrogen and sulphur atom interactions with the residual phenyl rings (CH $\cdots$ N and CH $\cdots$ S) and one CH $\cdots$ N interaction from the alkyl chain to the nitrile-nitrogen. (Fig. 4). One CH $\cdots$ CH contact supports the proximity of aliphatic chains of neighbouring molecules, namely C37–H37a $\cdots$ H42b–C42.

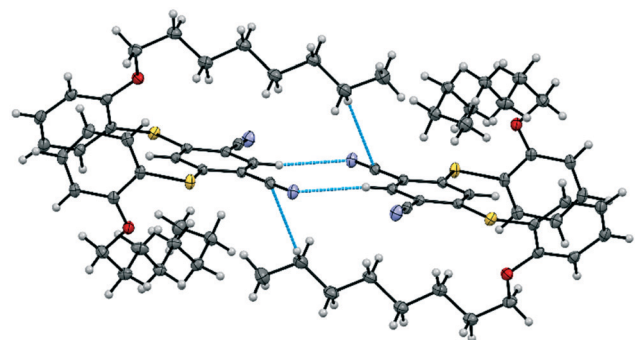


Fig. 3 Partial intermolecular landscape of *mNoP-C<sub>8</sub>* (CCDC Nr.: 1894901). Blue lines represent short intermolecular contacts below the sum of the van der Waals radii of the respective atoms. Color chart: grey = C, white = H, red = O, purple = N, and yellow = S. Ellipsoids are shown at the 50% probability level.

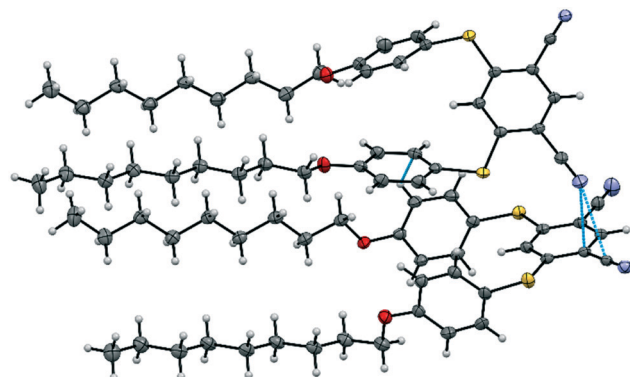


Fig. 4 Partial intermolecular landscape of *mNpP-C<sub>9</sub>* (CCDC Nr.: 1893331). Blue lines represent short intermolecular contacts below the sum of the van der Waals radii of the respective atoms. Color chart: grey = C, white = H, red = O, purple = N, and yellow = S. Ellipsoids are shown at the 50% probability level.

The structure of (Ox)*mNpP-C<sub>8</sub>* is almost identical to the one of *mNpP-C<sub>8</sub>* which we reported previously.<sup>7</sup> The interplanar angle of the phenyl rings is 39.5°, only slightly smaller compared to the one of 47.05°, which is present in the structure of *mNpP-C<sub>8</sub>* and seems geometrically unfavourable to generation of  $\pi\cdots\pi$  interactions. In the crystal packing an unsymmetrical dimer-like structure involving the non-classical C–H $\cdots$ N interactions between the central phenyl ring and one nitrile-nitrogen atom was found (C3A–H3A $\cdots$ N2B 2.571 Å; 157.0° and C3B–H3B $\cdots$ N1A 2.353 Å; 161.3°). This yields a layer with the alkyl chains on both sides. The dents in the layer's surface are filled with alkyl chains of the neighbouring layer. As a result, all molecules are oriented approximately parallel to [203] (Fig. 5). The second nitrile-nitrogen together

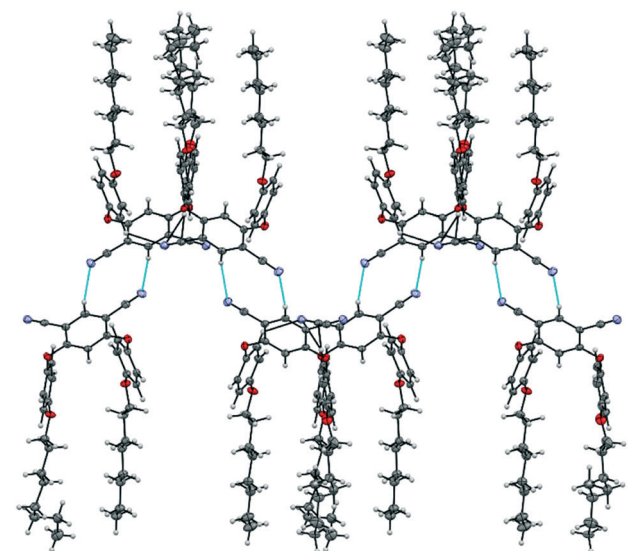


Fig. 5 Partial intermolecular landscape of (Ox)*mNpP-C<sub>8</sub>* (CCDC Nr.: 1895424). Blue lines represent short intermolecular contacts below the sum of the van der Waals radii of the respective atoms. Color chart: grey = C, white = H, red = O, and purple = N. Ellipsoids are shown at the 50% probability level.

with the adjacent oxygen atom from the central phenyl ring and with one C–H unit from one residual phenyl group is involved in the formation of hydrogen bond interactions with the neighbouring residual phenyl rings and one oxygen atom from the alkyl chain.

### In-depth packing analysis

Until now, we used only geometrical descriptors for the analysis of our structures. In this perspective, we identified short intermolecular contacts and described them as contributors to the overall crystal packing.<sup>7</sup> This geometrical description, although familiar to most chemists and easy to understand, is sometimes misleading for determining structure–property relationships from the analysis of intermolecular interactions. The reason for this is that the given distance is not necessarily equal to the energy minimum, a fact that does not hold even for strong hydrogen bonds.<sup>19</sup> More rigorous arguments have been invoked by other authors, namely the change in the electronic interaction between molecules, as a consequence of the formation of the postulated intermolecular bond as detected experimentally by spectroscopic methods.<sup>20</sup> Even in this case, the relative hierarchy of the intermolecular bond in the solid-state packing remains, however, undetermined. In the present discussion, we shift the focus from atom–atom contacts to the analysis of molecule–molecule bonding in terms of electron density, showing that the geometry is a poor substitute for energy. Therefore, a reference molecule in the crystalline packing was defined (as provided by CrystalExplorer) and then molecule pairs with surrounding molecules were analysed with respect to their intermolecular interactions. In this respect we selected the five most significant pairs (Fig. 6–8).

These pairs are called structure determinants and are identified by a color code, a symmetry operator joining the two molecules in the pair and by a distance between centers of mass. Full details about these quantities for each structure determinant are provided in the ESI†. In each structure determinant, the interaction energies are calculated with the CrystalExplorer “accurate” model scheme and decomposed in physically meaningful and familiar terms as described before (Fig. S5–S12, ESI† for each individual contribution).

***mNpP-C<sub>8</sub>***.<sup>7</sup> This is an excellent example showing how misleading a structural description based only on geometrical descriptors can be, especially when weak interactions are considered, thus requiring precise quantification based on quantum chemical calculations. The hierarchy of interaction energies is shown in Fig. 6A. Although no close contacts are detected from a geometrical inspection (below the sum of the van der Waals radii of the atoms in the considered molecules), by far the most important interaction is the one where both molecules are interacting due to the close proximity of four aromatic rings in the slipped stacked configuration, giving rise to strong  $\pi\cdots\pi$  interactions, which is in contrast to the geometric hints. This interaction mode is dominated by dispersion (see Fig. S5, ESI†) with a coulombic contribution

which is only 20% of the dispersive contribution. Another important mode ranks third in the hierarchy and was already discussed by our group as important from geometrical considerations. In this mode, edge-to-face  $\text{CH}_{(\text{arom})}\cdots\pi$  interactions are important, but one should not neglect the van der Waals interactions between neighbouring aliphatic chains, which again keep the coulombic contribution small (24% of the dispersion contribution). The non-classical hydrogen bonds formed by  $\text{CH}_{(\text{arom})}\cdots\text{N}$  interactions deserve special attention, since they are also observed in the (*Ox*)*mNpP-C<sub>8</sub>* structure. Although this interaction mode seems important from geometrical considerations, it only ranks sixth in the hierarchy (see Fig. S5 and S13, ESI†) and thus is excluded from the analysis. Only for this interaction mode the coulombic contribution dominates over the others.

***oNpP-C<sub>8</sub>***.<sup>7</sup> The main contribution to the crystal packing of this structure is the slipped stacked mode, where several favourable  $\pi\cdots\pi$  interactions between aromatic rings occur (Fig. 6B). This mode also supports segregation of the aliphatic chains from the aromatic cores, which bring the former in close proximity, giving rise to a strong, dispersion-dominated binding. A mode which we discussed already ranks third in our hierarchy (Fig. 6B); however, non-classical  $\text{CH}_{(\text{arom})}\cdots\text{N}$  hydrogen bonds play a very minor role here, in contrast to geometrical expectations. This is demonstrated by the very low contribution ( $-11.6\text{ kJ mol}^{-1}$ , Fig. S6, ESI†) of the coulombic interaction compared to the dispersion contribution ( $-63.7\text{ kJ mol}^{-1}$ , Fig. S6, ESI†).

***pNpP-C<sub>8</sub>***.<sup>7</sup> In this crystal structure, the most important interaction mode features a cyclic, non-classical, hydrogen-bonded dimer, which resembles the mode in *oNpP-C<sub>8</sub>* and (*Ox*)*mNpP-C<sub>8</sub>* (Fig. 6C). However, there are important differences among the three structures. Besides the two non-classical hydrogen bonds, the interaction mode of *pNpP-C<sub>8</sub>* also features  $\text{CH}_{(\text{alxyl})}\cdots\pi$  and  $\text{CH}_{(\text{alxyl})}\cdots\text{CH}_{(\text{alxyl})}$  interactions. The former could be identified by looking at the electrostatic potential mapped on the Hirshfeld surface (Fig. S14, ESI†), while the latter are van der Waals interactions and makes this interaction mode dominated by dispersion, despite the presence of two non-classical hydrogen bonds. At variance with the previously described structures, all interaction modes but one contribute similarly (within  $10\text{ kJ mol}^{-1}$ ) to the sum of interaction energies.

***pNoP-C<sub>8</sub>***. In this crystal structure the computational and geometrical descriptions are both accurate.

The first structure determinant in our hierarchy features strong  $\pi\cdots\pi$  interactions between the nitrile groups and the central phenyl rings as well as interactions between slipped stacked phenyl rings (Fig. 7A). The interaction mode which features  $\text{CH}_{(\text{arom})}\cdots\text{N}$  nonclassical hydrogen bonds ranks third, with a substantial – but not dominant – coulombic contribution.

***pNmP-C<sub>8</sub>***. Here a single interaction mode dominates all the others, namely the slipped stacked mode, which even from geometrical inspection is able to provide strong  $\pi\cdots\pi$  interactions (Fig. 7B). Despite the fact that electrostatic

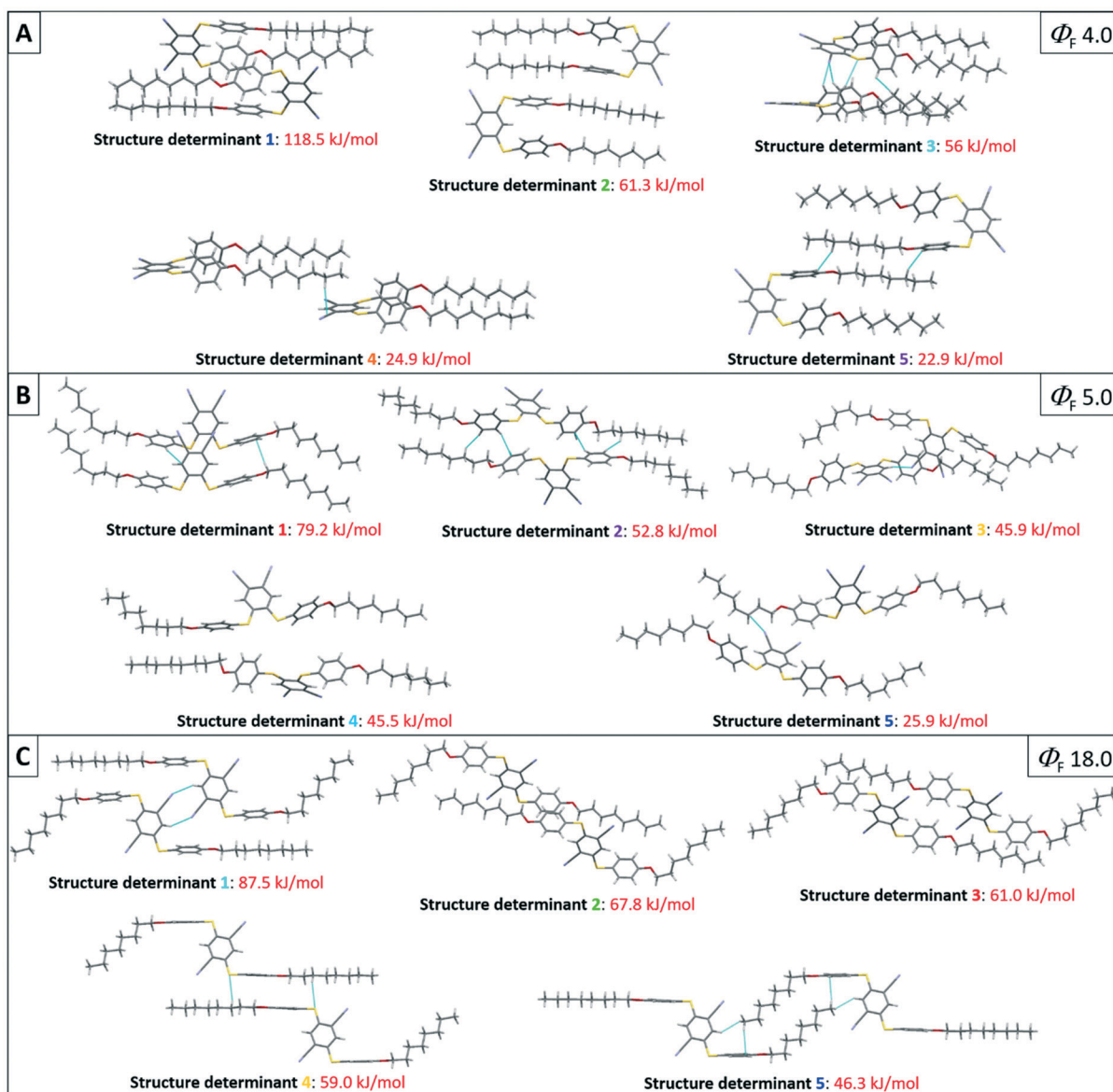


Fig. 6 Supramolecular hierarchy of the five most stabilizing interactions in the *mNpP-C8* structure (A), *oNpP-C8* structure (B) and *pNpP-C8* structure (C) as provided by CrystalExplorer. Blue lines represent short intermolecular contacts below the sum of the van der Waals radii of the respective atoms. Color chart: grey = C, white = H, red = O, purple = N, and yellow = S. Fluorescence quantum yields measured on the aggregates  $\Phi_F$  are given in %. For the color codes corresponding to each structure determinant see the ESI†

interactions are evident from the electrostatic potential mapped on the Hirshfeld surface (Fig. S15, ESI†), this interaction mode is also dominated by dispersion which contributes ( $191 \text{ kJ mol}^{-1}$ ) to the total interaction energy budget.

*mNoP-C8*. This structure is slightly disordered and we modelled it in the approximation that we are dealing with static disorder, so the disordered molecule can be in one conformation – or the other – in different cells. Both conformations gave the same hierarchy of structure determinants, with energy differences between the conformers which were small ( $1 \text{ kJ mol}^{-1}$ ), so only the major component is discussed here. We used the same strategy to model the (Ox)*mNpP-C8* structure which is discussed later. The two top ranking structure determinants of this crystal structure feature both electro-

static and dispersion terms (Fig. 8A). The cyclic hydrogen-bonded dimer of structure determinant 2 is very similar of that of other structures and is responsible for important electrostatic contribution, but dispersion interactions are ubiquitous and outrank by a factor of 2 the electrostatic contribution for both the interaction modes. All other structure determinants are dominated by dispersive forces.

*mNpP-C9*. This is another example highlighting the differences between the computational and geometrical descriptions, with the latter being more accurate. The first-ranked interaction mode is an almost pure van der Waals dimer. Even if no close contacts are detected here, the interactions among closely approaching alkyl chains, which are van der Waals in nature, are the main responsible for the binding. The

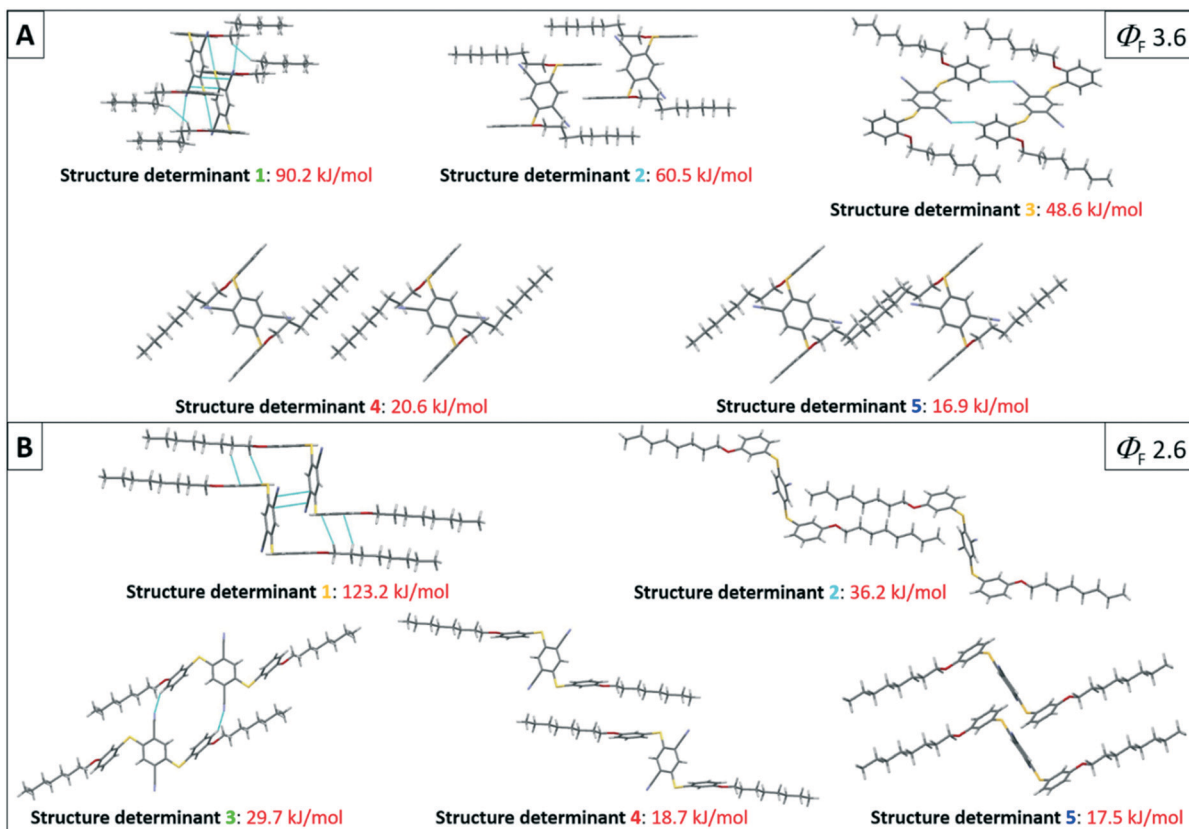


**Fig. 7** Supramolecular hierarchy of the five most stabilizing interactions in the *pNoP-C<sub>8</sub>* structure (A) and *pNmP-C<sub>8</sub>* structure (B) as provided by CrystalExplorer. Blue lines represent short intermolecular contacts below the sum of the van der Waals radii of the respective atoms. Color chart: grey = C, white = H, red = O, purple = N, and yellow = S. Fluorescence quantum yields measured on the aggregates  $\Phi_F$  are given in %. For the color codes corresponding to each structure determinant see the ESI.†

dispersion energy accounts for about 90% of the total energy of this structure determinant. Other important contributions to the crystal packing (equally ranked at about  $52 \text{ kJ mol}^{-1}$ ) are given by two structure determinants, featuring both  $\text{CH}_{(\text{alkyl})} \cdots \pi$  and  $\text{CH}_{(\text{alkyl})} \cdots \text{CH}_{(\text{alkyl})}$  interactions. In the first one (structure determinant 2), both electrostatics and dispersion give important contributions, while in the second one (structure determinant 3), dispersion strongly dominates (Fig. 8B).

**(Ox)*mNpP-C<sub>8</sub>*.** As discussed previously, this structure is, from visual inspection, very similar to the one of *mNpP-C<sub>8</sub>* (Fig. 8C). The structure is slightly disordered and we modelled it similarly to *mNoP-C<sub>8</sub>*. As shown previously for the *mNpP-C<sub>8</sub>* structure, the first-ranking structure determinant features no short contacts between both molecules, but a strong binding is given by the interactions among four slipped stacked aromatic rings and  $\text{CH}_{(\text{alkyl})} \cdots \pi$  interactions. The structure determinant, featuring non-classical hydrogen bonds formed by  $\text{CH}_{(\text{arom})} \cdots \text{N}$  interactions and shown in Fig. 5, is outranked by all the others as is observed for the *mNpP-C<sub>8</sub>* structure and is excluded from our discussion.

### Structure–property relationships

As we explained in the Introduction, we deal with molecules with restricted intramolecular rotations. The mechanism of

restriction of intramolecular rotations (RIR) was proposed by Tang and collaborators to explain the AIE behaviour of many classes of molecules.<sup>1b</sup> It has been described how massive  $\pi \cdots \pi$  slipped stacked interactions, which cause radiationless transitions, are detrimental to the AIE behaviour, while  $\text{CH} \cdots \pi$  interactions restrict the molecular motions of the phenyl rings, leading to increased AIE. Based on this mechanism we will qualitatively analyse the structure–property relationships of our systems supported by quantum chemical calculations. In Fig. 6 the compounds *mNpP-C<sub>8</sub>*, *oNpP-C<sub>8</sub>* and *pNpP-C<sub>8</sub>*, all with a *p*-substituted alkoxy chain, are compared and their fluorescence quantum yields (PLQYs) increase in the order *pNpP-C<sub>8</sub>*  $\gg$  *oNpP-C<sub>8</sub>* > *mNpP-C<sub>8</sub>*. Looking at Fig. 6A, in the packing of *mNpP-C<sub>8</sub>* the by far dominating structure determinant ( $\sim 118 \text{ kJ mol}^{-1}$ , twice the stabilization of the second highest-ranking mode) is the one which features four slipped stacked aromatic rings which strongly interact due to  $\pi \cdots \pi$  interactions. This interaction mode is highly detrimental to the AIE behaviour and explains why *mNpP-C<sub>8</sub>* features the lowest PLQY. *oNpP-C<sub>8</sub>* features a PLQY which is slightly higher than that of *mNpP-C<sub>8</sub>*. Again the most stabilizing structure determinant features prominent  $\pi \cdots \pi$  slipped stacked interactions between neighboring nitrile-bearing aromatic rings and alkoxy-bearing aromatic rings for a total stabilization of  $\sim 79 \text{ kJ mol}^{-1}$ . In this case the

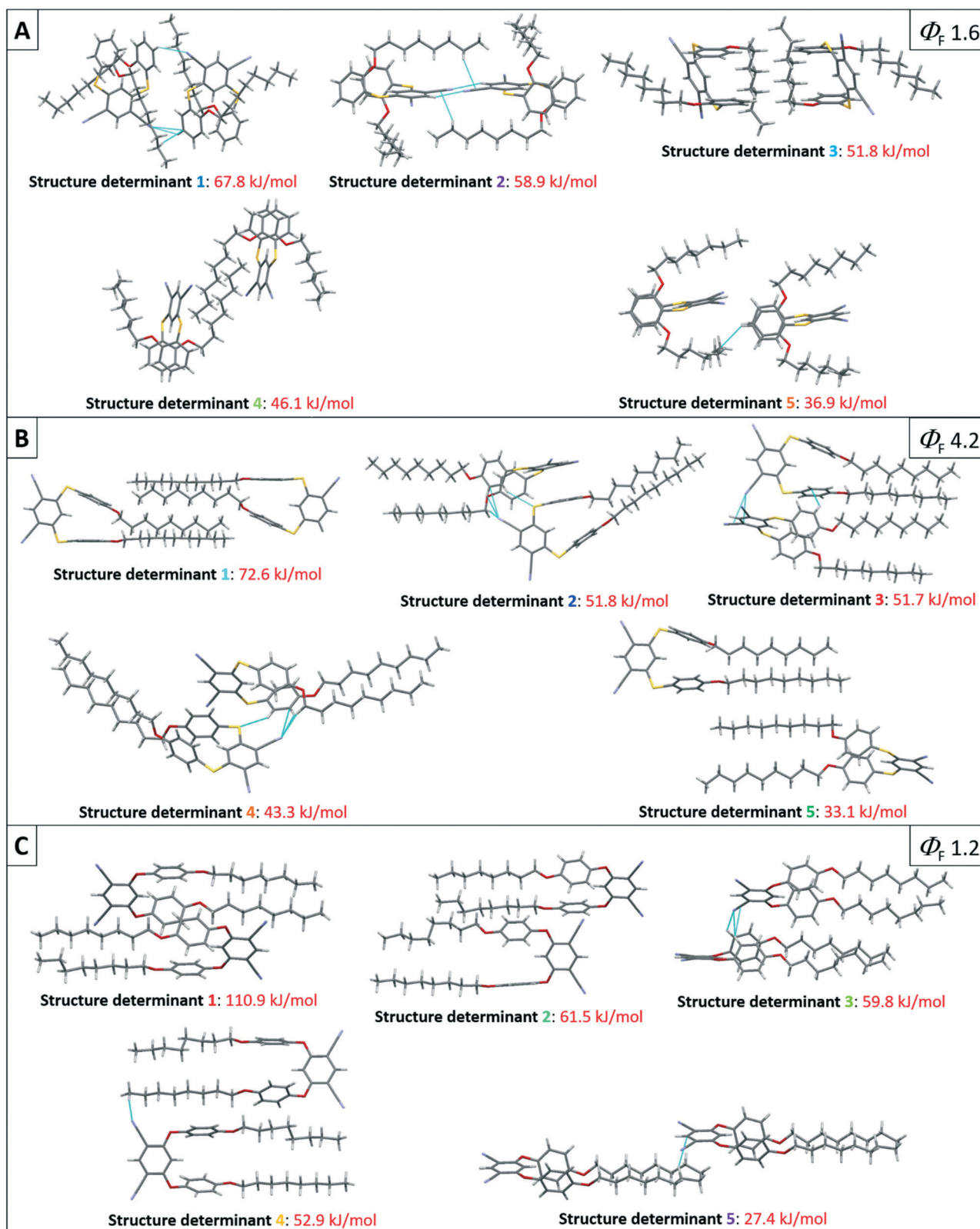


Fig. 8 Supramolecular hierarchy of the five most stabilizing interactions in the *mNoP-C8* structure (A), *mNpP-C9* structure (B) and *mNpP-C8* structure (C) as provided by CrystalExplorer. Blue lines represent short intermolecular contacts below the sum of the van der Waals radii of the respective atoms. Color chart: grey = C, white = H, red = O, purple = N, and yellow = S. Fluorescence quantum yields measured on the aggregates  $\Phi_F$  are given in %. For the color codes corresponding to each structure determinant see the ESI.†

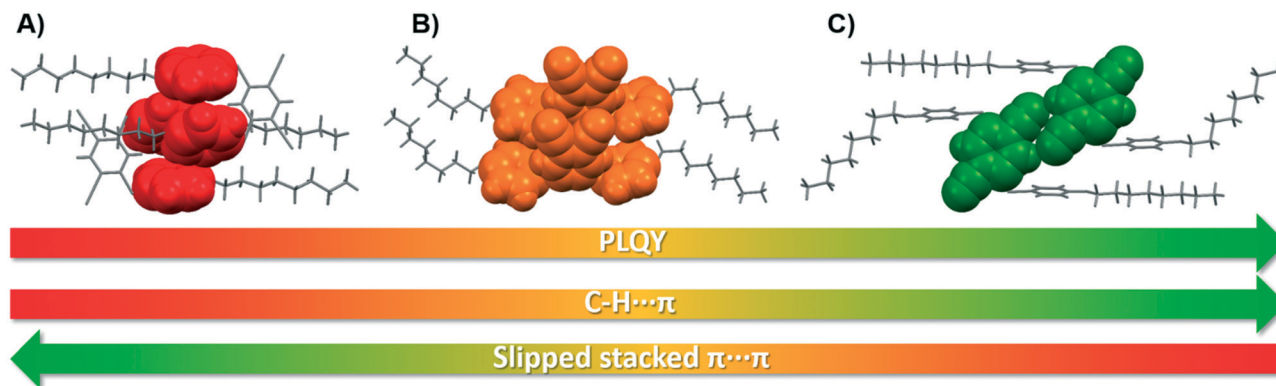


Fig. 9 Schematic view of the structure–property relationships derived from our in-depth packing analysis, A) compound *mNpP-C8*, B) compound *oNpP-C8*, C) and compound *pNpP-C8*.

contribution of the most stabilizing structure determinant is strong but not dominating, a fact that can explain the slightly higher PLQY for the *oNpP-C8* molecule. The case of *pNpP-C8* is very interesting: it features the highest PLQY of all the molecules within the investigated systems (Scheme 1). The first-ranked structure determinant features virtually no  $\pi\cdots\pi$  interactions, but relevant electrostatic forces ( $\sim 27$  kJ mol<sup>-1</sup>, see Fig. S7, ESI<sup>†</sup>) which we attribute to the formation of the cyclic non-classical hydrogen bond dimer (Fig. 6C). Important  $\text{CH}_{(\text{alxyl})}\cdots\pi$  and  $\text{CH}_{(\text{alxyl})}\cdots\text{CH}_{(\text{alxyl})}$  interactions give rise to strong dispersive forces which greatly stabilize the packing and restrict the rotational motions of the phenyl rings, giving a high PLQY. It is worth mentioning that all interaction modes but one contribute similarly (within 10 kJ mol<sup>-1</sup>) to the budget of interaction energies of *pNpP-C8* and no possible  $\pi\cdots\pi$  interactions are detected (except for structure determinant 4). Our findings are summarized in Fig. 9.

In Fig. 7 another comparison is made, namely that involving the *para*-nitriles, to which we include also *pNpP-C8* in Fig. 4C. The PLQYs increase in the order *pNpP-C8*  $\gg$  *pNmP-C8*  $>$  *mNoP-C8* which could be explained with the same arguments used for the series in Fig. 6. The structures in Fig. 8 deserve a separate discussion. *mNpP-C<sub>9</sub>* and (Ox)*mNpP-C<sub>8</sub>* were prepared with the purpose of investigating odd/even effects and single-atom-mutation, respectively, taking *mNpP-C<sub>8</sub>* as a reference. As explained before, due to the odd/even effects, the packing of *mNpP-C<sub>9</sub>* differs significantly to that of *mNpP-C<sub>8</sub>*, but their PLQYs are essentially the same, even if no direct  $\pi\cdots\pi$  slipped stacked interactions are found in the case of *mNpP-C<sub>9</sub>*. We attribute this behaviour to the fact that the first structure determinant (which does not feature  $\pi\cdots\pi$  slipped stacked interactions) contributes substantially to the interaction energy budget of this structure but it is not dominant (72.6 kJ mol<sup>-1</sup>). Other important structure determinants such as 2 and 4 (Fig. 6B) feature important  $\pi\cdots\pi$  interactions and explain the low PLQY for this molecule. The behaviour of (Ox)*mNpP-C<sub>8</sub>* is not easy to rationalize: the PLQY is much lower compared to that of *mNpP-C<sub>8</sub>* and the packing of both molecules is very similar. A possible difference is due to the presence of  $\text{CH}_{(\text{arom})}\cdots\text{S}$  interactions in *mNpP-C<sub>8</sub>* which re-

strict the molecular motions of the phenyl rings, leading to increased AIE (Fig. 6A, structure determinant 3). These interactions are not present in (Ox)*mNpP-C<sub>8</sub>* (Fig. 8A, structure determinant 3) and this could explain the lower PLQY.

## Conclusions

In conclusion, the present study aims to correlate the AIE behaviour of a series of luminophores with their structural features as observed in the solid state. Since AIE is a complicated phenomenon, with its interpretation being still under debate,<sup>1b</sup> our discussion is based on the well-established restriction of intramolecular rotation mechanism proposed by Tang and collaborators. In contrast to previous reports, our study includes, besides the classical discussion of intermolecular distances, an in-depth analysis of the crystalline packing supported by computational methods.<sup>14</sup> This analysis revealed that the enhancement of the fluorescence quantum yield is related to the significant increase of C–H $\cdots\pi$  and the decrease of  $\pi\cdots\pi$  interactions. Our investigation contributes to a better understanding of the photo-physical properties of AIE luminophores and the underlying intermolecular forces, which is crucial for the molecular design of functional materials.

## Conflicts of interest

There are no conflicts to declare.

## Acknowledgements

M. S. is gratefully indebted to Mark A. Spackman for suggestions on the modelling of disorder with CrystalExplorer. He thanks Angelo Gavezzotti, Peter Schwerdtfeger and Georg Jansen for discussions. MG thanks the Professor-Werdelmann Foundation and the “Fonds der chemischen Industrie” for generous financial support. J.V., J.S. and S.R. gratefully acknowledge the “Fonds der chemischen Industrie” for funding”. Jörg Rust and Christian W. Lehmann and the Petra III Beamline P11 at DESY are acknowledged for the determination of the X-ray structure of compound *pNmP-C<sub>8</sub>*.

## Notes and references

- 1 (a) Y. Hong, J. W. Y. Lam and B. Z. Tang, *Chem. Soc. Rev.*, 2011, **40**, 5361–5388; (b) J. Mei, N. L. C. Leung, R. T. K. Kwok, J. W. Y. Lam and B. Z. Tang, *Chem. Rev.*, 2015, **115**, 11718–11940.
- 2 (a) Z. P. Shields, J. S. Murray and P. Politzer, *Int. J. Quantum Chem.*, 2010, **110**, 2823–2832; (b) M. Saccone, G. Cavallo, P. Metrangolo, A. Pace, I. Pibiri, T. Pilati, G. Resnati and G. Terraneo, *CrystEngComm*, 2013, **15**, 3102–3105.
- 3 C. R. Martinez and B. L. Iverson, *Chem. Sci.*, 2012, **3**, 2191–2201.
- 4 J. Luo, Z. Xie, J. W. Y. Lam, L. Cheng, H. Chen, C. Qiu, H. S. Kwok, X. Zhan, Y. Liu, D. Zhu and B. Z. Tang, *Chem. Commun.*, 2001, 1740–1741, DOI: 10.1039/B105159H.
- 5 M. Hayduk, S. Riebe and J. Voskuhl, *Chem. – Eur. J.*, 2018, **24**, 12221–12230.
- 6 (a) B. Schmidt, S. Sankaran, L. Stegemann, C. A. Strassert, P. Jonkheijm and J. Voskuhl, *J. Mater. Chem. B*, 2016, **4**, 4732–4738; (b) S. Riebe, C. Vallet, F. van der Vight, D. Gonzalez-Abradelo, C. Wölper, C. A. Strassert, G. Jansen, S. Knauer and J. Voskuhl, *Chem. – Eur. J.*, 2017, **23**, 13660–13668; (c) J. Stelzer, C. Vallet, A. Sowa, D. Gonzalez-Abradelo, S. Riebe, C. G. Daniliuc, M. Ehlers, C. A. Strassert, S. K. Knauer and J. Voskuhl, *ChemistrySelect*, 2018, **3**, 985–991.
- 7 S. Riebe, M. Saccone, J. Stelzer, A. Sowa, C. Wölper, K. Soloviova, C. A. Strassert, M. Giese and J. Voskuhl, *Chem. – Asian J.*, 2019, **14**, 814–820.
- 8 A. J. Stone, in *Non-Covalent Interactions in Quantum Chemistry and Physics*, ed. A. Otero de la Roza and G. A. DiLabio, Elsevier, 2017, pp. 3–26, DOI: 10.1016/B978-0-12-809835-6.00002-5.
- 9 P. Schwerdtfeger, R. Tonner, G. E. Moyano and E. Pahl, *Angew. Chem., Int. Ed.*, 2016, **55**, 12200–12205.
- 10 B. Paulus, K. Rosciszewski, N. Gaston, P. Schwerdtfeger and H. Stoll, *Phys. Rev. B*, 2004, **70**, 165106.
- 11 J. Řezáč and P. Hobza, *Chem. Rev.*, 2016, **116**, 5038–5071.
- 12 (a) B. Jeziorski, R. Moszynski and K. Szalewicz, *Chem. Rev.*, 1994, **94**, 1887–1930; (b) K. Szalewicz, *WIREs Comput. Mol. Sci.*, 2012, **2**, 254–272; (c) G. Jansen, *WIREs Comput. Mol. Sci.*, 2014, **4**, 127–144.
- 13 (a) R. Dovesi, A. Erba, R. Orlando, C. M. Zicovich-Wilson, B. Civalleri, L. Maschio, M. Rérat, S. Casassa, J. Baima, S. Salustro and B. Kirtman, *WIREs Comput. Mol. Sci.*, 2018, **8**, e1360; (b) J. Hutter, M. Iannuzzi, F. Schiffmann and J. VandeVondele, *WIREs Comput. Mol. Sci.*, 2014, **4**, 15–25; (c) P. Blaha and S. B. Trickey, *Mol. Phys.*, 2010, **108**, 3147–3166; (d) J. Hafner, *J. Comput. Chem.*, 2008, **29**, 2044–2078.
- 14 A. Gavezzotti, *Top. Curr. Chem.*, 2012, **315**, 1–32.
- 15 (a) A. Gavezzotti, *J. Phys. Chem. B*, 2002, **106**, 4145–4154; (b) A. Gavezzotti, *J. Phys. Chem. B*, 2003, **107**, 2344–2353.
- 16 M. J. Turner, J. J. McKinnon, S. K. Wolff, D. J. Grimwood, P. R. Spackman, D. Jayatilaka and M. A. Spackman, *CrystalExplorer17*, University of Western Australia, 2017, <http://hirshfeldsurface.net>.
- 17 M. J. Turner, S. Grabowsky, D. Jayatilaka and M. A. Spackman, *J. Phys. Chem. Lett.*, 2014, **5**, 4249–4255.
- 18 S. P. Thomas, P. R. Spackman, D. Jayatilaka and M. A. Spackman, *J. Chem. Theory Comput.*, 2018, **14**, 1614–1623.
- 19 E. D’Oria and J. J. Novoa, *CrystEngComm*, 2004, **6**, 368–376.
- 20 G. A. Jeffrey, *An introduction to hydrogen bonding*, Oxford university press, New York, 1997.